VALIDATION OF A NUMERICAL METHOD FOR DETERMINING LINER IMPEDANCE

Willie R. Watson*

NASA Langley Research Center, Hampton Virginia

Michael G. Jones†

Lockheed Engineering & Sciences Company, Hampton Virginia

Sharon E. Tanner‡ And Tony L. Parrott‡

NASA Langley Research Center, Hampton Virginia

Abstract

This paper reports the initial results of a test series to evaluate a method for determining the normal incidence impedance of a locally reacting acoustically absorbing liner, located on the lower wall of a duct in a grazing incidence, multi-modal, nonprogressive acoustic wave environment without flow. This initial evaluation is accomplished by testing the methods' ability to converge to the known normal incidence impedance of a solid steel plate, and to the normal incidence impedance of an absorbing test specimen whose impedance was measured in a conventional normal incidence tube. The method is shown to converge to the normal incident impedance values and thus to be an adequate tool for determining the impedance of specimens in a grazing incidence, multi-modal, nonprogressive acoustic wave environment for a broad range of source frequencies.

Nomenclature

$[A(\zeta)], [A_I], [B_I]$	=complex block tridiagonal matrices
$[A^{[I,J]}]$	=local element matrix
a, b	=length and height, respectively, of a finite element
c_0, ρ_0	= ambient sound speed and density, respectively
d	=cavity depth
$E(\varsigma, \eta)$	=field equation error function
$EW(\varsigma)$	=wall error function
f	=frequency in Hertz
$f_1(\varsigma), f_2(\varsigma)$	=one dimensional basis functions
$\{F\}$	=vector containing source effects

---

*Research Scientist, Aerodynamic and Acoustics Method Branch, Fluid Mechanics Division.
†Principal Engineer, Research Division.
‡Research Scientists, Structral Acoustics Branch, Fluid Mechanics and Acoustics Division.

H, L	=height and length respectively, of the impedance tube test section
I, J	=axial and transverse node numbers
$IMAX, JMAX$	=number of points in the resistance and reactance grid,respectively
i	=$\sqrt{-1}$
k	=free space wavenumber
L_1, L_2	=the leading and trailing edge, respectively, of the test specimen
M, N	=number of nodes in the x and y direction, respectively
N_1, N_2, N_3, N_4	=two dimensional basis functions
m	=number of upper wall measurement points
$p(x, y)$	=complex acoustic pressure at (x, y)
p_1, p_2, p_3, p_4	=complex acoustic pressure at local nodes 1,2,3, and 4, respectively
p_{ref}	=reference pressure $(20\mu\mathrm{Pa})$
$p_s(y), p_{wall}$	=acoustic source and wall pressure, respectively
SPL	=measured sound pressure in decibels
x, y	= cartesian coordinates
$x_1, x_2, \ldots x_m$	=locations of upper wall microphones
β	=$\xi + i\sigma$, dimensionless admittance
$\{\Phi\}$	= global vector of the complex acoustic pressure
$\{\Phi^{[I,J]}\}$	= local vector of the complex acoustic pressure
ϕ	=measured phase angle for the complex acoustic pressure
ζ	=$\theta + i\chi$, dimensionless wall impedance
$\zeta_{exit}(y)$	= dimensionless exit impedance
η, ς	= local coordinate system for a finite element

1 Introduction

Highly efficient duct treatments for acoustic noise suppression continue to be a critical consideration in the achievement of environmentally acceptable commercial aircraft. To this end, a continuing concern in treatment technology is the accurate determination of the normal incidence impedance of an acoustic material underneath the boundary layers of grazing flows. Methods for determining the normal incidence impedance in such environments typically fall into three categories, "T-tube" method (refs. [1]), "in-situ" method (refs. [2, 3]), and the "propagation model" methods. All three methods have advantages and disadvantages, depending on facilities available, instrumentation and test liner construction or complexity. The disadvantages of the "T-tube" and "in-situ" methods are summarized in ref. [4]. These two methods do, however, serve as useful complements to the "propagation model" method, which is the subject of this paper.

The propagation model method is operationally convenient for extracting impedance spectra of test specimens in grazing flow environments. Consequently, flow duct facilities have been designed in an attempt to obtain the appropriate environment for duct propagation models. The current procedure is to use an infinite-wave-guide propagation model to extract the impedance of the test specimen from the measured data (i.e., spatial attenuation and phase rates on walls opposite the test liner) for a single, unidirectional propagating mode (refs. [4, 5, 6, 7]). However, in real facilities, these idealized test conditions (i.e., uni-

directional, single propagating mode) generally are attained only in an approximate manner under the best of laboratory conditions, and typically degrade severely with increasing mean flow. Additionally, many conventional test liner structures, and, in particular, the innovative liner structures currently under investigation, generate complex acoustic fields because of scattering of energy into higher order modes. While this may be a desirable result from the standpoint of achieving more efficient, broadband absorbing structures, it is a complicating feature that cannot be handled by the traditional unidirectional, single mode propagation model method.

In a recent paper (ref. [8]), a method for extracting the acoustic impedance of a material installed as a finite length wall segment of a duct carrying a nonprogressive multi-modal sound field in the absence of flow was presented. The method was shown to be successful for an assumed infinite liner using analytically based input data. The purpose of this paper is to validate the impedance extraction method using measured data and a finite length liner. More specifically, the impedance extraction method developed in ref. [8] is validated by testing the ability of the method to reproduce known normal incidence impedance data for a solid steel plate and a sound absorbing specimen. In contrast to the analytically based input data used in ref. [8], all input data used in this report were obtained from acoustic pressure measurements taken in a grazing incidence impedance tube facility with the test specimen installed.

The remainder of this paper is organized into five sections. Section 2 describes the measurement system used to obtain the input data for the numerical method and gives a brief description of each test specimen. The governing equations and boundary conditions are presented in section 3. Section 4 describes the numerical method which is used to extracts the unknown impedance. The known normal incidence impedances for the specimen was used as a baseline against which the accuracy of the model is judged. These results are presented in section 5. Finally, conclusions relevant to this paper as well as ongoing research activities are presented in section 6.

2   Experimental Set-Up and Test Specimens

The input data used to extract the impedance of each test specimen was obtained from measurements using a flow impedance tube in the NASA Langley Flow Impedance Laboratory. This multi-configurational apparatus has a 51x51 mm cross-section and is designed to produce a controlled aeroacoustic environment with a Mach number of up to 0.6 over a test specimen length of 41 cm. Four 120-watt phase-matched acoustic drivers generate signals over a frequency range of 0.3 to 3.0 kHz, with sound pressure levels up to 155 dB at the test specimen leading edge. In the present investigation there was no mean flow. Sound pressure levels of at least 120 dB at each frequency of interest were set at the leading edge of the test specimen. A schematic of the flow impedance tube is provided in figure 1. The test section (the section of the duct between the source and exit plane) is 84 cm long. The upper and two side walls of the test section are stainless steel.

Acoustic waves are propagated from left to right, across the surface of the test specimen, and into a termination section designed to minimize reflections over the frequency range of interest. Two 6 mm condenser-type microphones were flush-mounted in the test section,

one at a fixed location on the side wall, and the other on an axial traverse bar. A 13 mm wide precision-machined slot in the top wall of the flow impedance tube allows this axial traverse bar to traverse the test section length by means of a computer controlled digital stepping motor. The fixed location microphone was used to provide a reference for phase measurements. The data acquisition program automatically positioned the traversing microphone at a number of pre-selected locations ranging from 18 cm upstream of the leading edge to 52 mm downstream of the trailing edge of the test specimen. At each measurement location a transfer function between the traversing and the fixed microphone was measured and used to determine the sound pressure level and phase relative to the fixed microphone. The complex acoustic pressure at the wall location is determined from the equation

$$p_{wall} = p_{ref} 10^{\frac{20}{SPL}} e^{i\phi} = p_{ref} 10^{\frac{20}{SPL}} [\cos \phi + i \sin \phi] \tag{1}$$

A block diagram of the electronic instrumentation and signal conditioning system is given in figure 2. At each test frequency, a sound pressure level was set at the test specimen leading edge with a signal generator.

The duct propagation model, which is discussed in the following section, requires a measurement of three sets of input data

(1) The upper wall acoustic pressures

(2) The source plane acoustic pressure

(3) The exit plane impedance

Unfortunately, the source plane acoustic pressure and exit plane impedance are functions of position along these planes. Therefore, transverse probe microphones should be used to measure this data when the test specimen is installed. However, a transverse probe microphone was not available for this initial investigation. The experiment was therefore carefully designed, so as to minimize higher order mode effects along the source and exit boundary. All data for the duct propagation model was therefore be obtained from measurements made by the upper wall traversing microphone. It should be noted that because of the sound absorbing properties of the liner, it is not possible to avoid higher order mode effects in the liner region. In addition, higher order mode effects and reflections will occur in the vicinity of the leading and trailing edge of the specimen.

In order to avoid the use of a transverse probe, the source plane was chosen 18 cm upstream (3.5 duct diameters) of the leading edge of the test specimen in the hardwall section of the duct, and the source frequency was kept below the cuton of higher order hardwall modes. Higher order mode effects caused by the installation of the test specimen are expected to decay upstream of the leading edge of the test specimen. Therefore, the source pressure at each point along the source plane was set to the value measured at the upper wall source location.

A Similar procedure was applied at the exit plane. The exit plane was located 25 cm downstream (5 duct diameters) of the trailing edge of the test specimen, also in the hardwall section of the duct. The method developed in ref. [9] was used, with a hardwall test specimen installed to obtain the exit impedance. This was done by measuring complex acoustic pressures at five locations along the top wall of the impedance tube using the axial traverse

bar mounted microphone. The same exit impedance was used for both the hardwall and the conventional liner configurations. Because the exit plane is 5 duct diameters downstream of the trailing edge of the liner and higher order modes are cutoff, higher order modes generated by the installation of the liner are not expected to carry appreciable acoustic energy to the exit plane. Thus, the exit impedance values at all points along the exit plane were set to that obtained at the upper wall.

Input data were obtained for two specimens. The first specimen was a stainless steel plate (hardwall test specimen) for which the impedance was known. The second (a sound absorbing specimen) was a conventional uniform liner that consisted of a 100 MKS Rayl fibermetal facesheet bonded to a 100 mm deep aluminum hexcell honeycomb structure backed by a rigid plate. This type of liner construction has been used by the aeronautics industry for at least 35 years. Installed, this test specimen spanned the 51 mm width of the test section for a length of 41 cm. Normal incidence impedance measurements for this sound absorbing specimen were obtained using a conventional normal incidence impedance tube measurement, identical to that used in ref. [9]. Because of the simplification that the absence of mean flow affords, these measured normal incidence impedances and the impedances predicted using the method described in this report (using grazing incident sound) are expected to compare favorably. Thus, the measured normal incidence impedance is used as a baseline against which to judge the accuracy of the impedance extraction method when flow is absent.

3   Governing Equation And Boundary Conditions

In this section a brief description of the governing equation and boundary conditions used to extract the impedance of each test specimen is presented. Figure 3 depicts the applicable geometry and coordinate system used to model the test section of the Langley Impedance Tube. The axial and transverse directions are denoted by x and y, respectively. The spanwise direction, normal to the (x, y) plane, is not shown in the figure. To limit the propagation model to two dimensions, plane waves are assumed in the spanwise direction. This is a reasonable assumption since the sidewalls of the impedance tube are rigid and the sound frequency is below the cuton of any higher order modes. The lower and upper walls of the duct are located at $y = 0$ and $y = H$, respectively, and are also rigid except where the liner is located. The source and exit planes are located in the hardwall section of the duct at $x = 0$ and $x = L$, respectively. The test specimen (assumed locally reacting) is installed in the lower wall and has a normalized impedance, $\zeta = \theta + i\chi$. The leading and trailing edge of the specimen are at $x = L_1$ and $x = L_2$, respectively. To perform the computation for the hardwall baseline (i.e., the stainless steel plate) it is convenient to use the acoustic admittance of the specimen, defined as $\beta = \xi + i\sigma$. Measurement points are located along the upper wall at $x = x_1, x_2, x_3 \ldots x_m$ as shown. Acoustic pressure measurements at these locations were obtained with the traversing microphone as described in the previous section.

The mathematical problem is to find the solution to the Helmholtz equation

$$\frac{\partial^2 p(x, y)}{\partial x^2} + \frac{\partial^2 p(x, y)}{\partial y^2} + k^2 p(x, y) = 0 \tag{2}$$

Along the source plane of the duct ($x = 0$), the sound pressure level and phase of the acoustic pressure field is measured and expressed as a complex pressure, p_s, using equation (1). The

source plane boundary condition is therefore

$$p(0, y) = p_s \tag{3}$$

The boundary conditions along the rigid upper wall and the rigid portion of the lower wall are equivalent to the requirement that the gradient of the acoustic pressure normal to the wall vanishes

$$\frac{\partial p}{\partial y} = 0 \tag{4}$$

At the exit plane $(x = L)$, the ratio of acoustic pressure to axial velocity is assumed to equal the exit impedance

$$\frac{\partial p(L, y)}{\partial x} = \frac{-ikp(L, y)}{\zeta_{exit}} \tag{5}$$

Throughout this work, all impedances are normalized with respect to the characteristic impedance, $\rho_0 c_0$, of the air in the duct. Finally, the test specimen is assumed to be locally reacting, such that the boundary condition along the lower wall portion of the duct containing the test specimen is

$$\frac{\partial p}{\partial y} = \frac{ikp}{\zeta} \tag{6}$$

Equations (2)-(6) constitute a boundary value problem that can be solved to determine the unknown impedance, ζ, provided the upper wall pressure is known (ref. [8]). The solution for the unknown impedance can be put in terms of known functions only for special cases of the boundary conditions and upper wall pressure. These cases are not useful for general application. Therefore, the unknown impedance, ζ, must be determined by a numerical method for cases of practical interest.

4 The Numerical Method

The numerical method chosen to extract the unknown impedance of the lower wall is discussed in ref. [8] and only sufficient detail is presented here for continuity and completeness. Because the experimental set-up was designed to minimize higher order mode effects, the foregoing discussion will assume a constant source pressure, p_s, exit impedance, ζ_{exit}, and lower wall impedance, ζ. However, these functions need not be constants to successfully apply the method (ref. [8]). When applied to the current acoustic problem, the method may be interpreted as an approximation of the continuous acoustic field as an assemblage of rectangular finite elements as illustrated in figure 4. It is assumed that there are N nodes in the axial and M nodes in the transverse directions of the duct. A typical rectangular element, $[I, J]$, is shown in figure 5. Each element consists of four local node numbers labeled 1, 2, 3 and 4, respectively. Each element is considered to have width $a = (x_{I+1} - x_I)$ and height $b = (y_{J+1} - y_J)$ as shown. The objective of the method is to determine the impedance ζ, that minimizes the difference between the upper wall pressure obtained from the finite element solution, and that obtained from measured data with the specimen installed.

To begin, Galerkin's finite element method is employed to minimize the field error. The field error is distinct from the wall error function, which will be used to extract the unknown

impedance. First define the local coordinates, ς and η for the element

$$\varsigma = \frac{x}{a} \qquad\qquad \eta = \frac{y}{b} \qquad\qquad (7)$$

Now define the field error function as

$$E(\varsigma, \eta) = \frac{\partial^2 p(\varsigma, \eta)}{\partial \varsigma^2} + \frac{\partial^2 p(\varsigma, \eta)}{\partial \eta^2} + k^2 p(\varsigma, \eta) \qquad\qquad (8)$$

Within each element $p(\varsigma, \eta)$ is represented as linear combination of four functions, N_1, N_2, N_3 and N_4 which comprise a complete set of basis functions

$$p(\varsigma, \eta) = N_1(\varsigma, \eta)p_1 + N_2(\varsigma, \eta)p_2 + N_3(\varsigma, \eta)p_3 + N_4(\varsigma, \eta)p_4 \qquad\qquad (9)$$

$$N_1(\varsigma, \eta) = f_1(\varsigma)f_1(\eta) \qquad N_2(\varsigma, \eta) = f_2(\varsigma)f_1(\eta) \qquad\qquad (10)$$

$$N_3(\varsigma, \eta) = f_2(\varsigma)f_2(\eta) \qquad N_4(\varsigma, \eta) = f_1(\varsigma)f_2(\eta) \qquad\qquad (11)$$

$$f_1(\varsigma) = 1 - \varsigma \qquad\qquad f_2(\varsigma) = \varsigma \qquad\qquad (12)$$

In an ideal sense, the solution to the sound field is obtained when the field error, $E(\varsigma, \eta)$, is identically zero at each point of the domain. This is approximately achieved by requiring that the field error function be orthogonal to each basis function $N_I(\varsigma, \eta)$. Contributions to the minimization of the field error function from a typical element are

$$ab \int_0^1 \int_0^1 E(\varsigma, \eta)N_I(\varsigma, \eta)d\varsigma d\eta = [A^{[I,J]}]\{\Phi^{[I,J]}\} \qquad\qquad (13)$$

where $[A^{[I,J]}]$ is a 4x4 complex matrix for each element $[I, J]$, and $\{\Phi^{[I,J]}\}$ is a 4x1 column vector containing the unknown acoustic pressure at each of the four nodes of the element. The coefficients in the local matrix, $[A^{[I,J]}]$, were computed in closed form. It should be noted that the second derivative terms in the field error function, $E(\varsigma, \eta)$, were integrated by parts in order that linear basis functions could be used. Also, the wall and exit plane boundary conditions were substituted into these integrated terms.

Assembly of the global equations for the computational domain is a basic procedure in the finite element method. Appropriate shifting of rows and columns is all that is required to add the local element matrix, $[A^{[I,J]}]$, directly into the global matrix, $[A]$. Assembling the elements for the entire domain results in a matrix equation of the form

$$[A(\zeta)]\{\Phi\} = \{F\} \qquad\qquad (14)$$

where $[A(\zeta)]$ is a complex matrix whose order is MN, and $\{\Phi\}$ and $\{F\}$ are MNx1 column vectors. The vector $\{\Phi\}$ contains the nodal values of the unknown acoustic pressure and $\{F\}$ is the zero vector until the pressure source condition is imposed. It is necessary to apply the source condition to equation (14) before a solution can be obtained. Satisfying the noise source boundary condition consists simply of setting all nodal values of acoustic source pressure at the source plane to the known value of source pressure, this introduces nonzero elements into the first M components of $\{F\}$.

The global matrix $[A(\zeta)]$ generated by Galerkin's Method following application of the source condition is a complex symmetric matrix. Fortunately, owing to the discretization

7

scheme used, it will also be block tridiagonal. The structure of the matrix $[A(\zeta)]$ after imposing source conditions is shown in figure 6, where the superscript T denote matrix transpose. Note that $[A(\zeta)]$ is a square block tridiagonal matrix whose order is MN. This global matrix contains a number of major blocks (A_I, B_I) which are themselves square and block tridiagonal as shown in the figure. The matrix elements in each major block are computed explicitly in terms of the yet unspecified impedance, ζ. Much practical importance arises from this block tridiagonal structure as it is convenient for minimizing storage and maximizing computational efficiency. Special matrix techniques exist for a solution of this structure[1]. All computation and storage is performed only on the elements within the bandwidth of the matrix $[A(\zeta)]$.

The unknown impedance, ζ, of the acoustic material is determined from the measured upper wall acoustic pressure. The procedure is to determine the impedance ζ, such that the pressure along the top wall reaches its' measured value at each of the measurement points, x_I. The procedure consists of repeatedly cycling through the solution to equation (14), obtaining a set of upper wall pressures for each impedance value. As each new set of wall pressures is computed, it is compared to the measured value until convergence is achieved.

The idea is best illustrated as follows for a perforate. Define the unknown impedance as

$$\zeta = \theta + i\chi \tag{15}$$

where θ is the resistance and χ the reactance. Resistance values are positive whereas reactance values span the real axis

$$0 \leq \theta \leq \infty, \quad -\infty \leq \chi \leq \infty \tag{16}$$

It should be apparent that searching the entire upper half plane of the resistance/reactance space for the unknown impedance is impractical. Therefore, introduce the tranformation

$$\chi = \cot(kd), \quad 0 \leq kd \leq \pi \tag{17}$$

and search for the unknown impedance in the (θ, kd) plane, where θ is limited to, $0 \leq \theta \leq 10$, from practical considerations.

The complex plane, (θ, kd), is now divide into $IMAX$ evenly spaced intervals in the θ direction and $JMAX$ evenly spaced points in the kd direction, as shown in figure 7. The increment spacing $\Delta\theta$ and $k\Delta d$ are

$$\Delta\theta = \frac{10}{IMAX - 1}, \quad k\Delta d = \frac{\pi}{JMAX - 1} \tag{18}$$

Thus, a point $\zeta = \zeta_{IJ}$ in this uniform impedance grid is

$$\zeta_{IJ} = \theta_I + i\chi_J, \quad \theta_I = (I - 1)\Delta\theta, \quad \chi_J = \cot{(J - 1)k\Delta d} \tag{19}$$

If the measured upper wall pressures with the specimen installed are $p_{wall}(x_n, H)$, and those computed from the finite element solution with ζ replaced by ζ_{IJ} are $p(x_n, H)$, then a measure

---

[1]Gaussian elimination with partial pivoting and equivalent row infinity norm scaling is used to reduce the rectangular system to upper triangular form. Back substitution is then employed to obtain the solution for the acoustic pressure at the MN node points

of the closeness of ζ_{IJ} to ζ is given by the normalized wall error function, $EW(\zeta_{IJ})$

$$EW(\zeta_{IJ}) = \frac{\overline{EW}(\zeta_{IJ})}{\overline{E}_{max}} \qquad (20)$$

$$\overline{EW}(\zeta_{IJ}) = \frac{1}{m} \sum_{n=1}^{m} \mid p_{wall}(x_n, H) - p(x_n, H) \mid \qquad (21)$$

in which $\mid \; \mid$ denotes the absolute value of a complex quantity, $\overline{E}_{max}$ is the maximum value of $\overline{EW}$ for all points ζ_{IJ} in the impedance grid, and m is the number of known wall pressures.

Determining the unknown impedance of the material is now recast as a minimization problem. Thus, ζ should be chosen such that $EW(\zeta)$ is a global minimum. The global minimum is obtained using a two-step method. First, use a coarse grid in the impedance plane and tabulate the normalized wall error function to determine the location in that grid of an approximate minimum point (θ^1, kd^1). Next use a fine grid centered about (θ^1, kd^1) to obtain a new minimum. The location of the minimum point of this fine grid corresponds to the unknown impedance, ζ of the material. Coarse grid calculations are performed with $IMAX = 51$, $JMAX = 31$, and $\Delta\theta = k\Delta d = 0.1$. Fine grid calculations are carried out using $IMAX = JMAX = 21$, and $\Delta\theta = k\Delta d = 0.01$. The coarse and fine grid discretization were determined from numerical experimentation in an earlier work (ref. [8]).

5   Results

A computer code implementing the impedance extraction method has been developed. The finite element matrix equation (14) is solved using a routine a highly developed software package and minimization of the normalized wall error function is performed internally by an in-house computer code. The unknown impedance, ζ, is returned by the in-house code. Results were computed using a Dec-Alpha work station and were not computationally intensive (i.e., requiring only 0.5 seconds of CPU time for each point in the impedance grid). Analysis of the solid steel plate, for which the known admittance is zero ($\beta = \xi + \sigma i = 0 + 0i$) was conducted in the admittance plane for the sake of convenience. A 231x21 evenly spaced grid is used ($N = 231$ and $M = 21$) in the finite element discretization for all calculations. This grid ensured that a minimum of ten elements per axial wavelength was used in the finite element discretization at the highest frequency of interest.

Figure 8 shows a plot of the measured resistance and reactance of the normalized exit impedance as a function of frequency. Note that reflections are present in the test section since the resistance is not unity and the reactance has a non-zero value. Thus, the acoustic field in the Langley flow impedance tube is not purely progressive, even for the hardwall test specimen. The measured resistance and reactance spectrum of the exit impedance is tabulated in the second and third columns respectively, of table 1. Resistance values range from a minimum of 0.87 at 3,000 Hz to a maximum of 1.13 at 2,600 Hz. Reactance values range from a minimum of -0.12 at 2,800 Hz to a maximum of 0.12 at 2,300 Hz.

Hardwall admittance predictions using the method proposed in this study are shown first. The predicted normalized conductances, ξ, for the hardwall test specimen, are shown in figure 9. Predictions are shown for twenty-six frequencies ranging from 500 to 3,000 Hz,

in 100 Hz increments. The known and predicted conductance values are tabulated in the fourth and fifth columns, respectively, of table 1. The sixth column of table 1 is the error (the difference between the known and measured conductance values). The maximum error in the conductance prediction is only 0.02 (see tabulated results at 2,800 Hz). Figure 10 shows a graph of the predicted susceptance, σ. The predicted and known susceptances, truncated to two decimal digits of accuracy, were zero at each frequency; therefore, tabular results are not shown. Overall, the predictions for the conductance and susceptance using the measured input data appear as accurate as those predicted in ref. [8] for analytically based input data, with a solid surface installed.

An appropriate next step in the validation of the impedance extraction method is to install the conventional liner and predict the impedance of the soft test specimen. The liner and end effects will generate higher order modes and reflections in the test section that were not present for the solid steel plate. Figure 11 shows a comparison of the predicted and measured resistances, θ, for the conventional liner at six selected frequencies (500, 1,100, 1,500, 2,000, 2,500 and 3,000 Hz). Predicted and measured resistance values for the conventional liner are tabulated in the second and third columns, respectively, of table 2. Predicted resistance values range from a minimum of 0.39 at 500 Hz to a maximum of 0.72 at 2,000 Hz. At each frequency, the predictions are close to the measured values. A maximum error of -0.10 is observed in the resistance prediction at 1,500 Hz (see the fourth column of table 2). Figure 12 shows predicted and measured reactance comparisons for the conventional liner. The data for this graph are tabulated in the fifth and sixth columns of table 2. The variability in the reactance component of the impedance is noticeably greater than that of the resistance component. The maximum error in the predicted reactance is -0.20 and also occurs at 1,500 Hz (see column seven of table 2). Note that predicted reactance values are generally less accurate than the predicted resistance.

Since the largest error in the predicted and measured normal incidence impedance for the soft specimen occurred at 1,500 Hz, each impedance value was used to predict the attenuation of the soft test specimen with the prediction program. The attenuation predicted with the measured normal incidence impedance ($\zeta = .63 + 2.48i$) was 1.70dB and that obtained using the predicted impedance ($\zeta = .53 + 2.28i$) was 1.67dB. Thus, for the chosen soft test specimen, the diffence between the predicted and measured normal incidence impedance (i.e., .1 for resistance and -.2 for reactance) doesn't affect the overall noise reduction peformance of the test specimen.

Overall, resistance and reactance predictions with the liner installed match the measured normal incidence values quite well. However, the predictions are not as good as those obtained for the hardwall specimen. This is in contrast to the predictions obtained in ref. [8] with analytically based data, in which the predictions were just as accurate for soft as for rigid walls. There are several possible explanations as to why the predictions are less accurate with the liner installed when experimentally based input data is used. These are

(1) Twenty elements across the duct may not be sufficient to resolve the transverse acoustic field in the neighborhood of the discontinuties at the leading and trailing edge of the test specimen.

(2) Installation of the liner generates some transverse dependence in the acoustic field at either the source or exit plane (these effects have been neglected in the predictions).

(3) Differences between the predicted and measured values may be due to small errors in the measured normal incident impedance determination.

A more likely explanation is that a combination of these effects is responsible for slightly less accurate predictions when the liner is installed.

6   Conclusions and Discussion

A duct propagation model for extracting the acoustic impedance of a test specimen using measured data has been tested for effectiveness. Although the method as presented here does not contain flow effects, it is extendable to mean flows with shear. Results of this study show that the method is extremely effective in extracting the impedance of hard and soft specimens for a range of source frequencies. There is only a slight degradation in the accuracy of the impedance prediction when high quality measured data is used instead of analytically based data.

The results of this investigation represent a significant step in the development of a new and more complete impedance measurement technique. This method currently extends zero-flow impedance prediction capability to test specimens with non-uniform impedance distributions in nonprogressive acoustic wavefields, while maintaining impedance measurement accuracy. Additional validation experiments are planned, which should

(1) validate the measurement capability for more complicated sources and at higher frequencies

(2) validate the applicability of the method to variable impedance liners

Efforts are also underway to include the effects of shearing flows into the measurement technique. One important challenge in both the flow and zero-flow effort is to provide sufficiently accurate boundary condition data at the source and exit planes such as prescribed by equations (3) and (5). It will be recalled that in the source plane, the complex acoustic pressure distribution is required (and also the entrance impedance when flow is present) whereas in the exit plane the exit impedance distribution is required.

Presumably, the successful measurement of the complex pressures at two closely spaced planes would permit acoustic particle velocities to be inferred, thus permitting calculation of the exit or entrance plane impedance. Although fraught with difficulty, this approach is being actively pursued by the development of in-flow/out-flow acoustic probes to directly measure acoustic pressure distributions in both the source and exit planes. A second approach to acquiring source and exit plane pressure distributions is also being pursued. In this approach, acoustic pressure measurements are confined entirely to walls of the source and exit sections of the flow duct. These pressures are then used to 'construct' the inflow pressure and particle velocity fields from a modal decomposition of the hardwall pressure measurements. The advantages of this approach are

(1) the avoidance of in-flow or out-flow measurements

(2) the intuitive appeal and physical insight provided by the modal propagation model

References

[1] Feder, E., and Dean III, L.W.: "Analytical and Experimental Studies for Predicting Noise Attenuation in Acoustically Treated Ducts for Turbofan Engines," NASA CR-1373, 1969.

[2] Phillips, B., and Morgan, C. J.: "Mechanical Absorption of Acoustic Oscillations in Simulated Rocket Combustion Chambers," NASA TN D-3792, 1967.

[3] Phillips, B., 1967b "Effects of High Value Wave Amplitude and Mean Flow on a Helmholtz Resonator," NASA TMX-1582, 1967.

[4] Armstrong, D. L., Beckemeyer, R. J., and Olsen, R. F., "Impedance Measurements of Acoustic Duct Liners With Grazing Flow," Boeing paper presented at the 87th Meeting of the Acoustical Society of America, New York, NY, 1974.

[5] Watson, W. R.: "A Method for Determining Acoustic-Liner Admittance in a Rectangular Duct With Grazing Flow From Experimental Data," NASA TP-2310, 1984.

[6] Watson, W. R.: "A New Method for Determining Acoustic-Liner Admittance in Duct With Sheared Flow in Two Cross-Sectional Directions," NASA TP-2518, 1985.

[7] Parrott, T. L., Watson, W. R.,and Jones, M. G.:"Experimental Validation of a Two-Dimensional Shear-Flow Model for Determining Acoustic Impedance," NASA TP-2679, 1987.

[8] Watson, W. R., Jones M. G., Tanner, S.E., and Parrott, T. L.:"A Finite Element Propagation Model for Extracting Normal Incidence Impedance in Nonprogressive Acoustic Wave Fields," NASA TM-110160, April 1995.

[9] Jones, M. G., and Parrott, T. L.: "Evaluation of a Multi-point Method for Determining Acoustic Impedance," *Mechanical System and Signal Processing Journal*, vol. 3, no. 1, pages 15-35, 1989.

Frequency in Hz	Measured exit impedance		Conductance of the hardwall test specimen		
f	θ	χ	Known	Predicted	Error
500	1.03	0.02	0.00	0.01	0.01
600	0.97	0.03	0.00	0.01	0.01
700	1.05	-0.01	0.00	0.01	0.01
800	1.05	-0.01	0.00	0.00	0.00
900	1.03	-0.06	0.00	0.00	0.00
1,000	0.98	-0.04	0.00	0.00	0.00
1,100	0.98	-0.03	0.00	0.00	0.00
1,200	0.94	0.02	0.00	0.00	0.00
1,300	0.97	0.07	0.00	0.00	0.00
1,400	1.01	0.05	0.00	0.00	0.00
1,500	1.02	0.06	0.00	0.00	0.00
1,600	1.11	0.01	0.00	0.01	0.01
1,700	1.05	-0.05	0.00	0.01	0.01
1,800	1.04	-0.06	0.00	0.00	0.00
1,900	0.95	-0.10	0.00	0.01	0.01
2,000	0.92	-0.05	0.00	0.00	0.00
2,100	0.91	0.02	0.00	0.00	0.00
2,200	0.92	0.06	0.00	0.00	0.00
2,300	0.99	0.12	0.00	0.00	0.00
2,400	1.07	0.07	0.00	0.00	0.00
2,500	1.10	0.08	0.00	0.01	0.01
2,600	1.13	-0.07	0.00	0.01	0.01
2,700	1.05	-0.11	0.00	0.01	0.01
2,800	0.99	-0.12	0.00	0.02	0.02
2,900	0.90	-0.10	0.00	0.01	0.01
3,000	0.87	0.00	0.00	0.01	0.01

Table 1: Exit plane impedances and wall conductance values for the hardwall test specimen.

Frequency in Hz	Resistance of the conventional liner			Reactance of the conventional liner		
f	Predicted	Measured	Error	Predicted	Measured	Error
500	0.39	0.44	-0.05	-0.55	-0.66	0.11
1,100	0.46	0.40	0.06	-0.68	-0.61	-0.08
1,500	0.53	0.63	-0.10	2.28	2.48	-0.20
2,000	0.72	0.73	-0.01	-1.37	-1.47	0.10
2,500	0.53	0.45	0.08	0.09	0.17	-0.08
3,000	0.42	0.49	-0.07	1.35	1.30	0.05

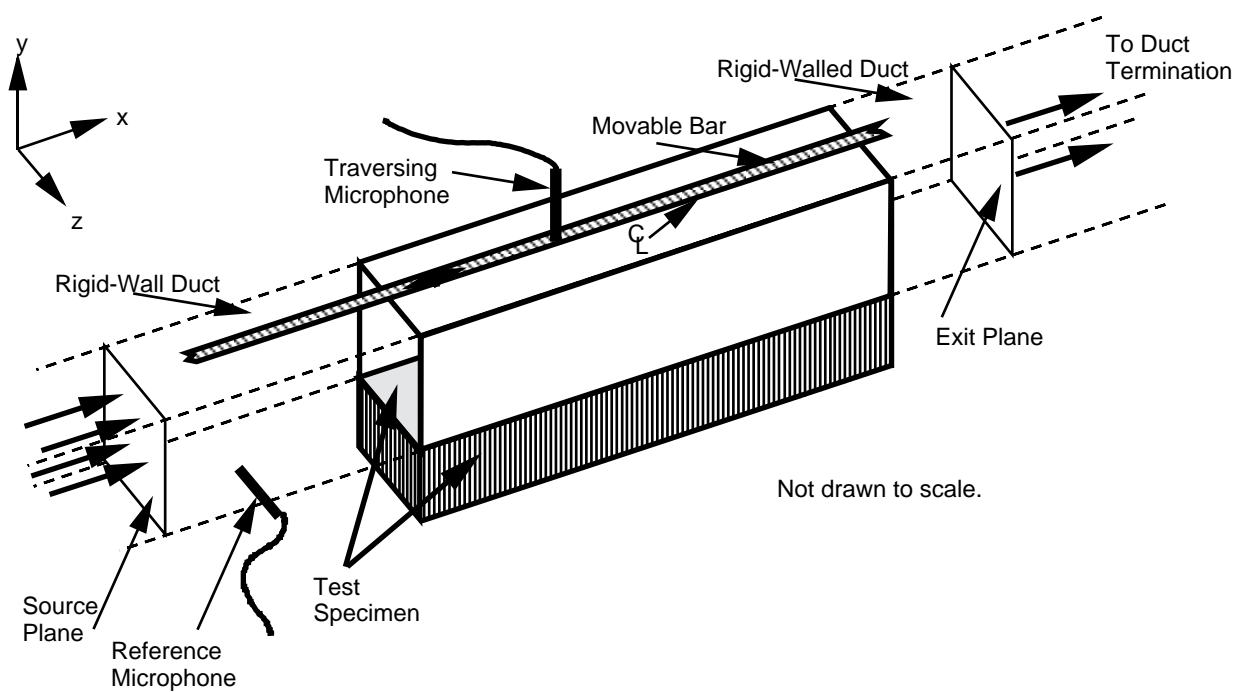Table 2: Predicted and measured impedance for the conventional liner.

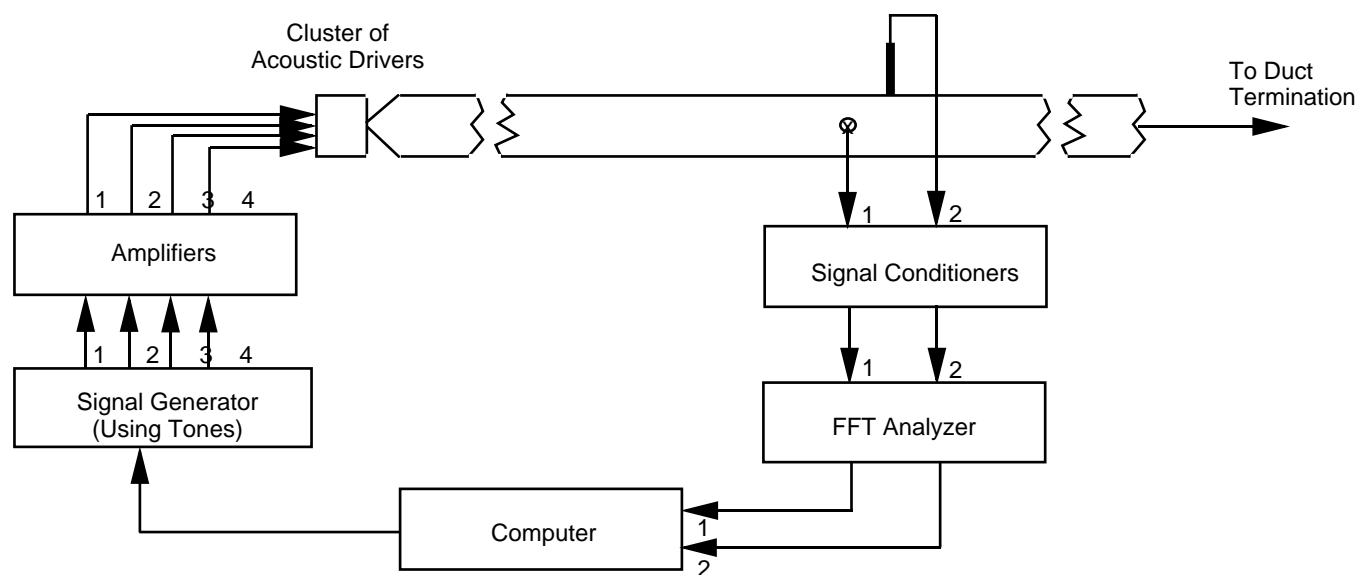Figure 1: Schematic of the Langley Flow Impedance Tube.

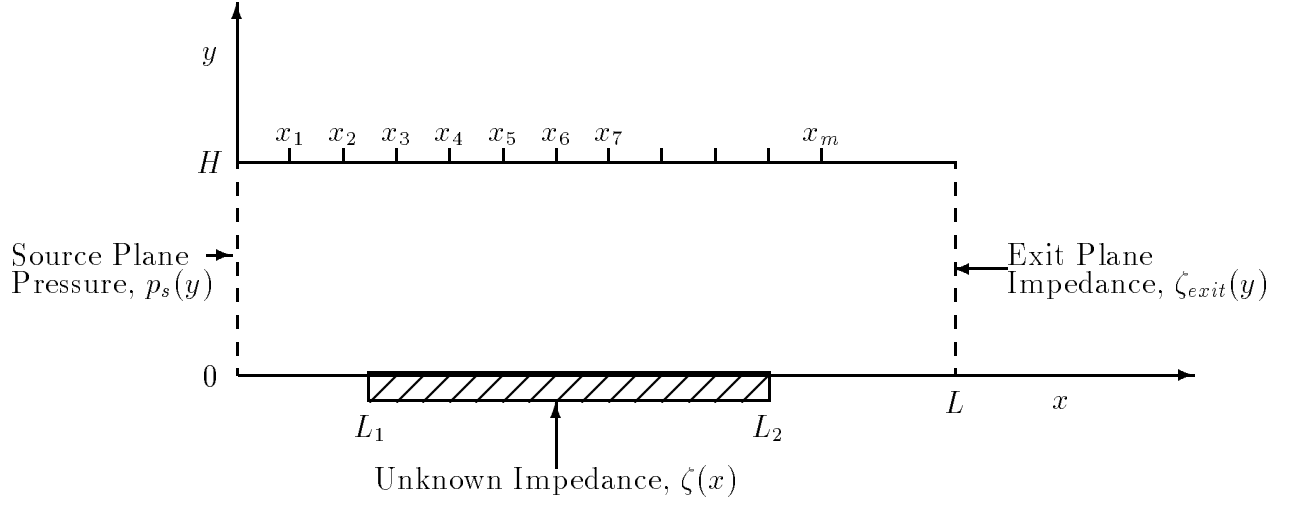Figure 2: The electronic instrumentation and signal conditioning system for the Flow Impedance Tube.

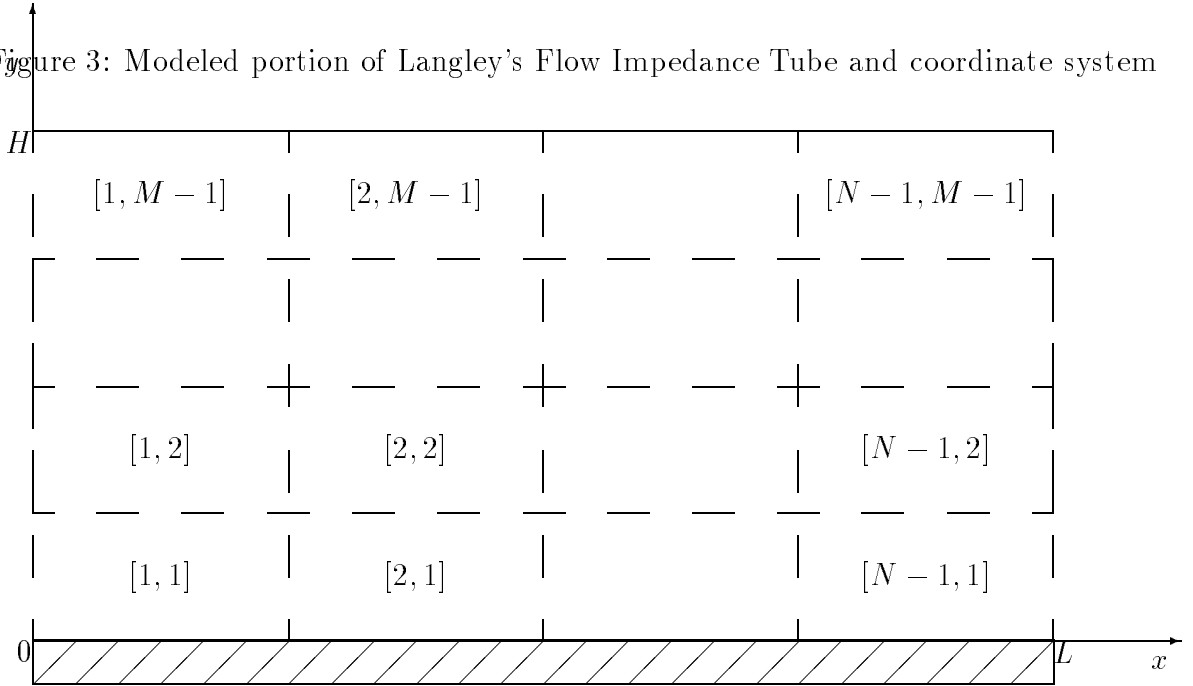Figure 3: Modeled portion of Langley's Flow Impedance Tube and coordinate system

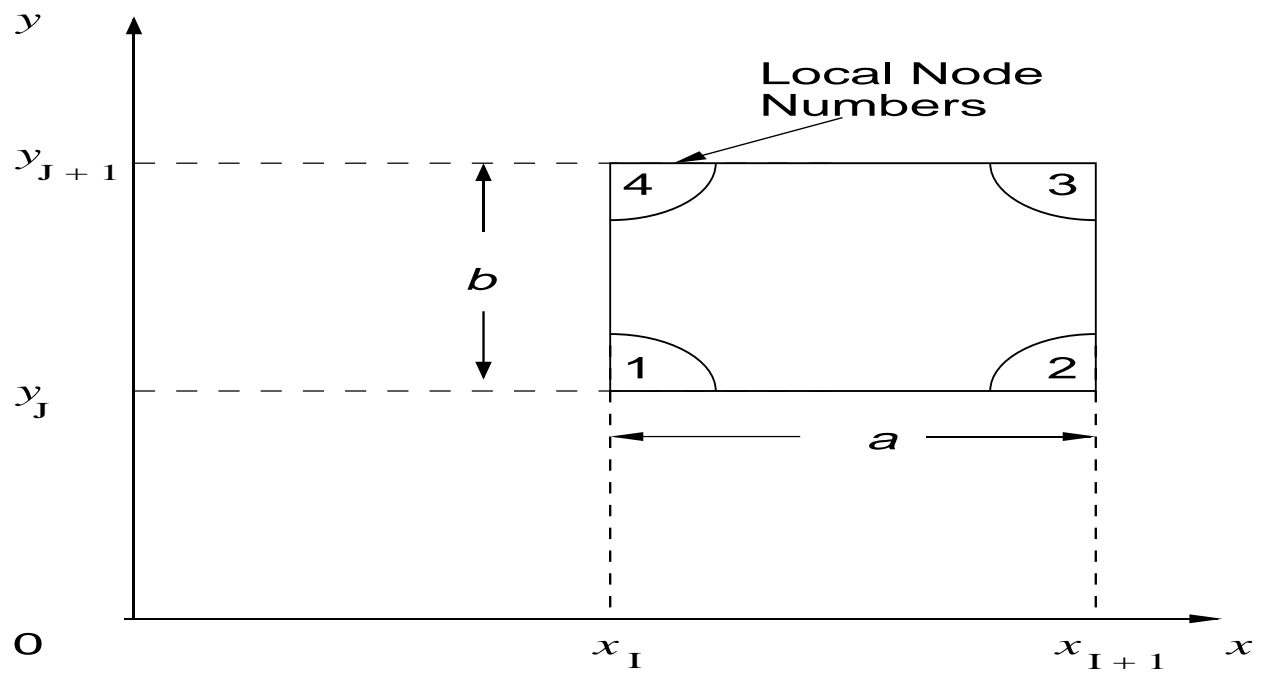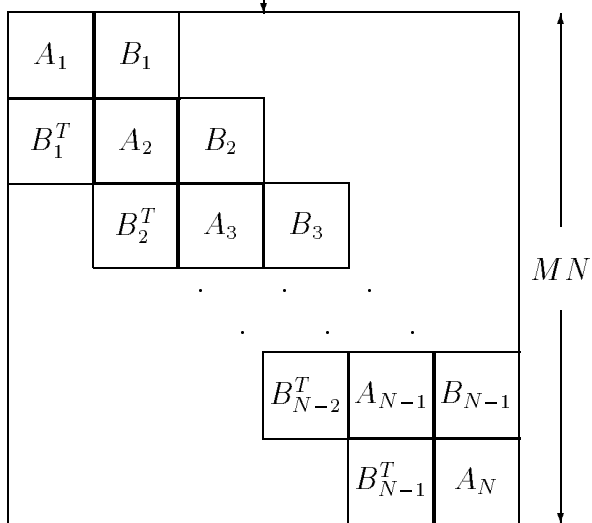Figure 4: Finite element discretization of two dimensional duct

Figure 5: A typical finite element, $[I, J]$, and local node numbering system

Structure of the global stiffness matrix
with major blocks, A_I, B_I and B_I^T

Structure of each major block,
each x is a complex number
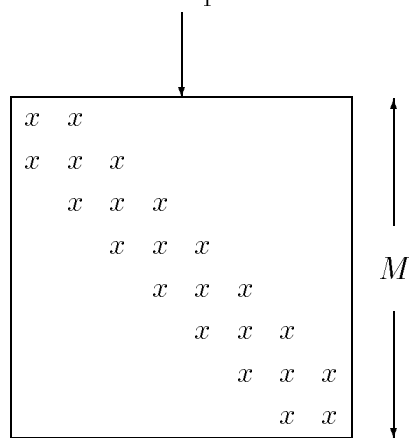
Figure 6: Structure of the global matrix and major blocks

Figure 7: Impedance grid in the complex plane
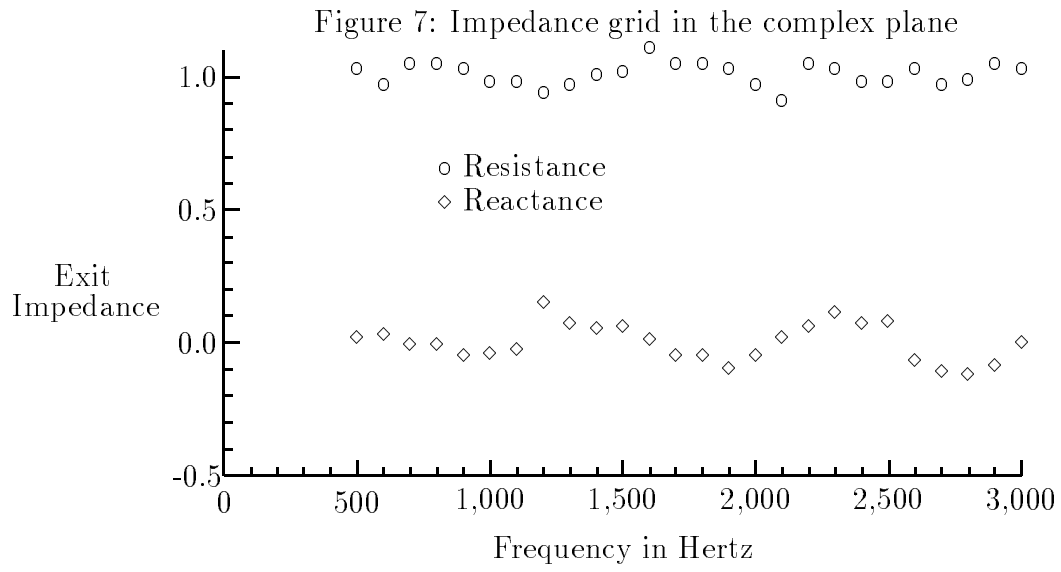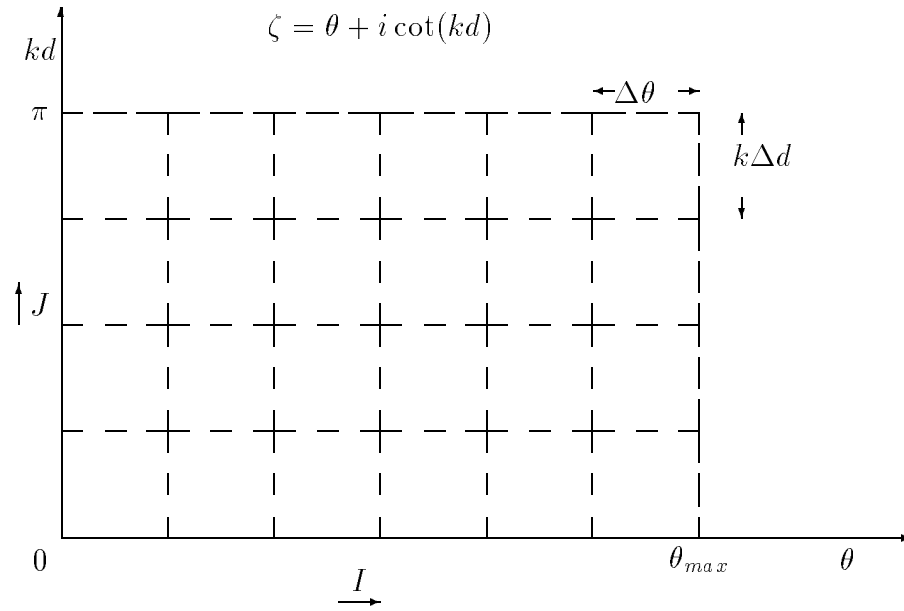
Figure 8: Measured exit impedance for the Langley Flow Impedance Tube.
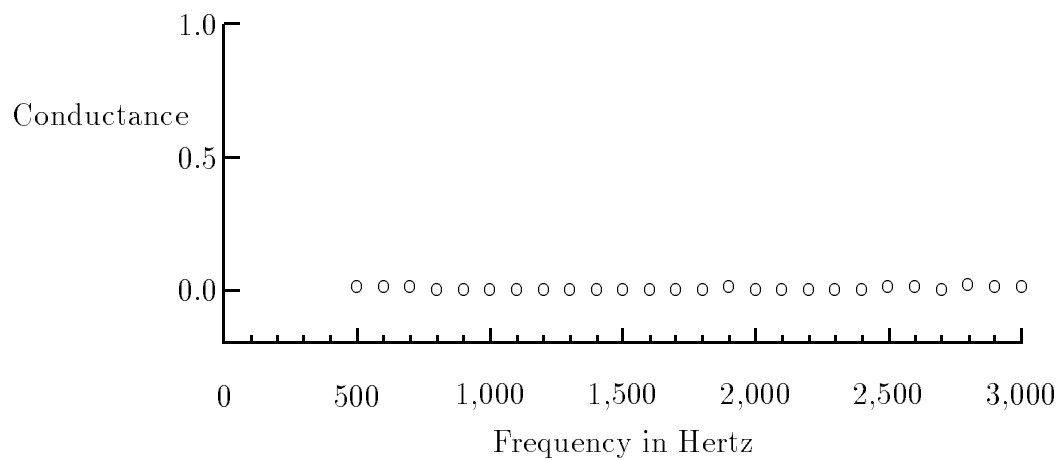
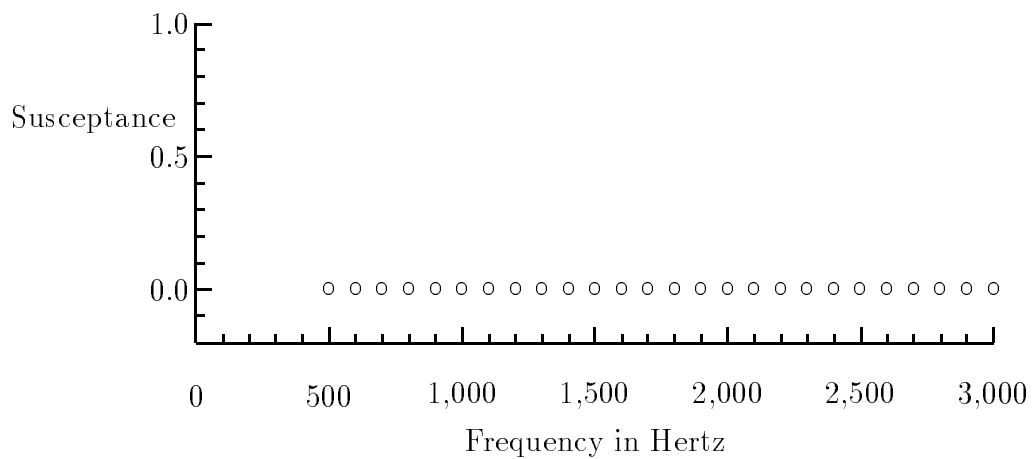Figure 9: Predicted conductance for the hardwall test specimen.

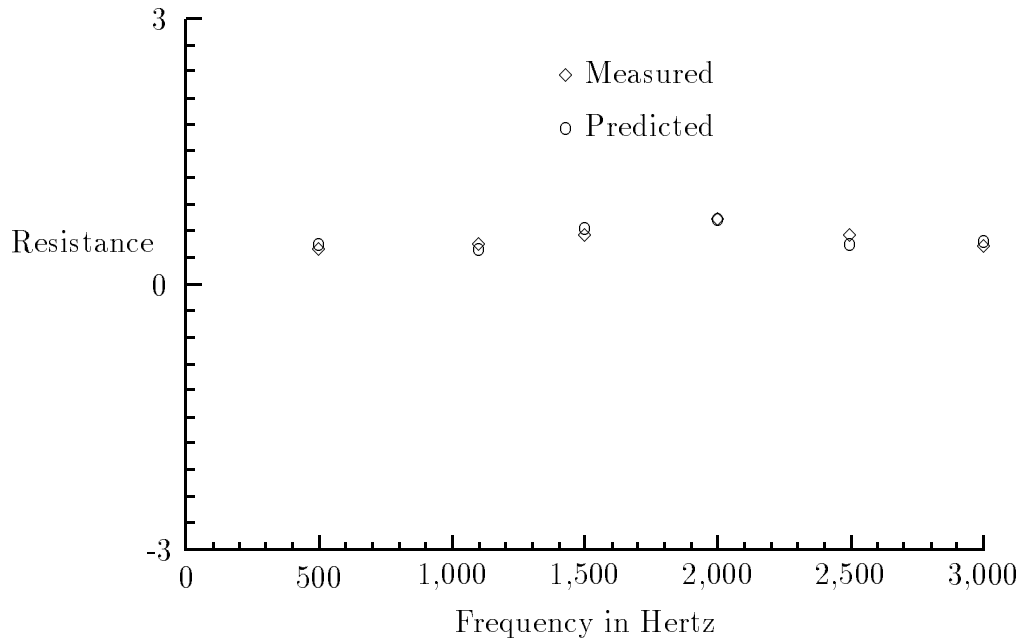Figure 10: Predicted susceptance for the hardwall test specimen

19

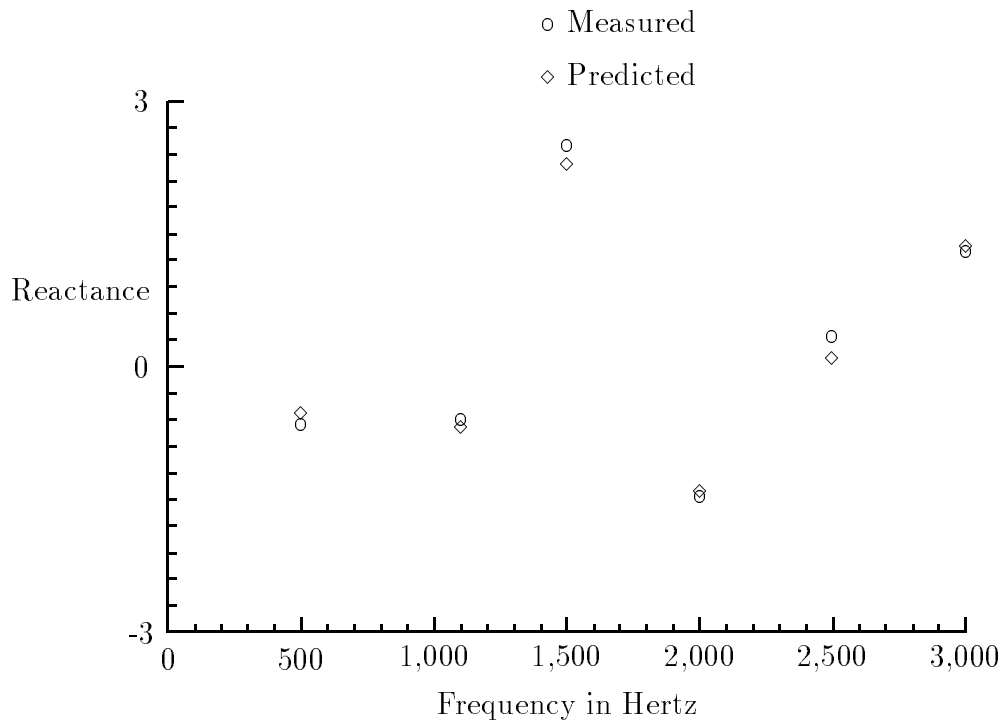Figure 11: Comparison of measured and predicted resistance for the conventional liner.

Figure 12: Comparison of measured and predicted reactance for the conventional liner